

## Risk Evaluation for Earth-fill Dams due to Heavy Rains - Probability of Failure due to Heavy Rains -

K. Kuribayashi<sup>1</sup>, N. Tanaya<sup>2</sup>, S. Kuroda<sup>3</sup>, T. Kato<sup>4</sup>, T. Tateishi<sup>5</sup>, R. Hirata<sup>6</sup>, T. Shibata<sup>7</sup> and S. Nishimura<sup>8</sup>

<sup>1</sup>Eight-Japan Engineering Consultants Inc. Email: kuribayashi-ke@ej-hds.co.jp

<sup>2</sup>Eight-Japan Engineering Consultants Inc. Email: tanaya-na@ej-hds.co.jp

<sup>3</sup>Eight-Japan Engineering Consultants Inc. Email: kuroda-shu@ej-hds.co.jp

<sup>4</sup>Eight-Japan Engineering Consultants Inc. Email: kato-to@ej-hds.co.jp

<sup>5</sup>Okayama Univ. Email: plb65pc0@s.okayama-u.ac.jp

<sup>6</sup>Okayama Univ. Email: pic80qzl@s.okayama-u.ac.jp

<sup>7</sup>Okayama Univ. Email: tshibata@cc.okayama-u.ac.jp

<sup>8</sup>Okayama Univ. Email: theg1786@okayama-u.ac.jp

**Abstract:** In recent years, many small earth-fill dams have collapsed due to heavy rains. Local governments, managing a large number of these dams, have been forced to formulate a rational policy for measures to counteract heavy rains. In this study, a risk assessment method, in which the probability of failure and the damage costs are identified, is proposed to determine the priority of the measures. In terms of the damage modes for earth-fill dams, two primary modes are examined, namely, the overflow of the reservoir and the slip failure at the downstream face of the dam. In the former case, the inflow into the dam due to rainfall is calculated, taking the catchment area and the land-use conditions at the upstream of the dam into consideration. A check is made as to whether the inflow exceeds the discharge capacity of the existing spillway. In the latter case, the safety factor of the slope in relation to the assumed rainfall is calculated by a saturated-unsaturated seepage analysis, and a stability analysis is done based on the circular slip surface. As a result, the return periods, corresponding to the expected dam failure, are obtained for 10 dams of different sizes. Evaluations to prioritize the countermeasures to heavy rains for earth-fill dams have traditionally been based only on the damage loss at the downstream area. This study proposes a method that includes the probability of failure along with the damage loss.

**Keywords:** Earth-fill dams, Risk evaluation, Rainfall, Seepage analysis.

### 1. Introduction

Heavy rain in July 2018 caused the breaching of 32 small earth-fill dams, principally in Hiroshima Prefecture, resulting in massive damage to housing and farming fields in the downstream area (MAFF 2018). Based on this experience, the Ministry of Agriculture, Forestry and Fisheries has reviewed the prioritization of small earth-fill dams from the viewpoint of disaster prevention and has formulated several countermeasures to safeguard such dams from heavy rains. However, it is unrealistic, in terms of costs and time, to try to implement perfect countermeasures for a huge number of small earth-fill dams, and the local governments managing these dams have been forced to formulate rational policies to conduct measures to counteract heavy rains.

This study proposes a risk assessment method for determining the priority of such measures for small earth-fill dams managed by local governments. In conventional approaches, the priority has been determined by calculating the damage loss that would be caused by the breach of each earth-fill dam in its downstream area. In contrast, the present study proposes an index of risks derived from the probability of damage and the costs of this damage for each earth-fill dam.

Damage to an earth-fill dam usually occurs in one of the three modes shown in Fig. 1 (Hori 2005). The first mode is “seepage failure caused by piping inside the dam embankment”. This mode of damage can often be attributed to the non-uniformity of the bank material. However, it is difficult to identify the safety against

seepage failure, because cases have been confirmed for which the existence of several piping holes was not the cause of the breach of the dam embankment. The second mode is “slip failure of the dam embankment”. Many past cases of this mode of breach have involved the seepage of rainwater into the downstream slope of the dam embankment, raising the water level inside the dam embankment and reducing the strength of the bank material. The third mode is “breach due to the overflow of the reservoir”. The flow of stored water over the crest erodes the downstream face of the slope, dissecting the cross section of the dam embankment.

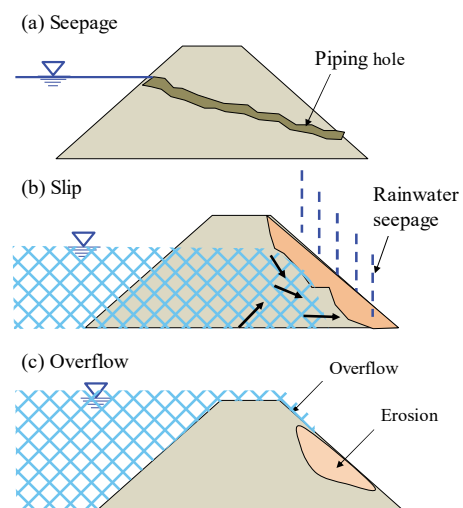


Figure 1. Damage modes of earth-fill dams in heavy rain

The damage probability is calculated in this paper for the second mode, “slip failure of the dam embankment”, and the third mode, “breach due to overflow of the reservoir”. For the former, the safety factor of the dam embankment can be calculated using an unsaturated seepage flow analysis, taking the seepage of the rainwater into consideration, and the circular slip surface calculation. For the latter, the inflow to a reservoir is calculated based on the catchment area and land-use conditions in the upstream area of the dam. In cases where the calculated inflow exceeds the discharge capacity of the existing spillway, overflows are assumed to occur.

## 2. Methods

### 2.1 Evaluation Procedure

The procedure for calculating the damage probability of a small earth-fill dam is shown in Fig. 2. To enable this calculation, the cross-section shape of the dam, the geological conditions of the dam and the foundation ground, the design discharge of the dam, and the discharge capacity of the spillway were obtained. The probability of precipitation was then calculated for each targeted small earth-fill dam. For this calculation, rainfall data observed in the vicinity of each dam were required, namely, the actual data on the maximum rainfall in each year of the observation period and the rainfall hyetograph of the greatest rainfall in the past. A cumulative probability distribution curve of the maximum rainfall data for each observation year was prepared. Then, the precipitation for each of the set return periods (for example, once in 100 years) could be obtained. The rainfall time series for the heaviest rainfall in the past was used as the base waveform and a hyetograph was prepared for each return period.

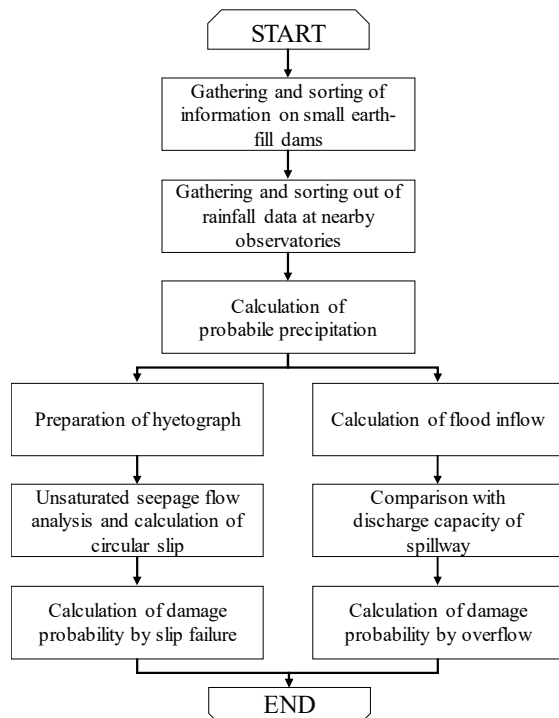


Figure 2. Evaluation flow diagram

Using these probabilistic hyetographs, an unsaturated seepage flow analysis was conducted to establish the changes in the water level inside the dam embankment. Meanwhile, the slope safety factor of the dam embankment was calculated for different water level conditions at different hours and then the time history of the safety factor against slip failure was calculated. This was followed by calculating the damage probability for the slip failure of the dam based on the minimum safety factor for each return period. Moreover, the flood inflow corresponding to the return period of each dam was calculated based on the maximum rainfall of each observation year. The probability of damage by overflow was calculated by comparing the calculated flood inflow with the discharge capacity of the dam's spillway.

### 2.2 Selection of Small Earth-Fill Dams

The small earth-fill dams targeted in this study were 10 dams of different sizes and catchment areas among existing dams located in Hiroshima Prefecture, where dams were actually damaged by heavy rain in July 2018. The parameters of the selected dams are shown in Table 1, which also lists the nearest rainfall observatory of the Japan Meteorological Agency (JMA) to each dam. The rainfall data obtained by the nearest JMA observatory were used for the preparation of a hyetograph for each dam.

Table 1. Object dams and rainfall observatories (JMA)

	Height (m)	Total volume of water (m <sup>3</sup> )	Catchment area (km <sup>2</sup> )	JMA rainfall observatory
A dam	10.0	66,210	0.320	Kure
B dam	9.0	155,400	0.200	Kure
C dam	26.0	255,000	2.500	Shiwa
D dam	5.5	21,600	0.720	Yawata
E dam	9.3	49,600	0.193	Tsushima
F dam	6.3	13,700	0.709	Miiri
G dam	4.7	1,019	0.230	Hiroshima
H dam	9.1	6,040	0.540	Hiroshima
I dam	9.9	27,868	0.030	Shiwa
J dam	6.5	3,100	0.010	Kure

### 2.3 Preparation of Hyetographs

A probabilistic hyetograph was prepared for each assumed return period using the rainfall observation data obtained from the JMA rainfall observatory near each dam. Firstly, a cumulative probability distribution curve of the maximum daily rainfall at each observation site was prepared using data observed in the past. Three probability distribution curves were employed, namely, the Gumbel distribution based on the extreme value distribution, the square root index-type maximum distribution (SqrtEt), and the generalized extreme value distribution (Gev) (MLIT 2014), and the maximum value of the probabilistic daily precipitation was found for each site. Table 2 shows the types of cumulative probability distribution curves, which fit the observed data well, and the maximum value of the daily probabilistic precipitation at each rainfall observatory. Each probability value was corrected by the Jackknife method to remove any

influence of singular values presumed to be included in the original data set (Takara et al. 1988).

From the prepared probability distribution curves, the maximum daily probabilistic precipitation was extracted corresponding to the return periods of 10, 50, 100, 200, and 400 years. The hyetograph for each return period was calculated using Eq. 1.

$$I_{prob}(t) = \frac{I_{probD}}{I_{obsD}} I_{obs}(t) \quad (1)$$

where  $I_{prob}(t)$ : probabilistic hyetograph,  $I_{obs}(t)$ : observed hyetograph,  $I_{probD}$ : probabilistic daily precipitation shown in Table 2 (mm/day), and  $I_{obsD}$ : maximum observed daily precipitation (mm/day).

As each observed hyetograph was based on a calculation, the hyetograph which had the largest amount of daily rainfall during the observation period at each observatory was adopted. The probabilistic hyetograph for each observation site is given in Fig. 3.

Table 2. Daily precipitation corresponding to return periods at each observatory

JMA rainfall observatory	Probability distribution curve	Daily precipitation (mm/day)				
		10 years	50 years	100 years	200 years	400 years
Kure	SqrEt	154	216	245	276	308
Shiwa	SqrEt	161	229	260	291	325
Yawata	SqrEt	223	320	366	414	465
Tsushima	Gumbel	170	229	254	278	303
Miiri	Gumbel	173	227	250	273	296
Hiroshima	SqrEt	158	219	248	278	310

#### 2.4 Calculation Method of Damage Probability

Two types of damage probability, namely, damage probability due to slip failure and damage probability due to overflow, were calculated. The former damage probability was calculated in the following manner. Firstly, the changes in the reservoir water level with the time series were calculated by the nonstationary unsaturated seepage flow analysis of rainwater seepage using the probabilistic hyetograph prepared for each dam. As the next step, a circular slip calculation was conducted for the earth-fill dam by considering the changes in the subsurface water level. Following this procedure, the time series of the safety factor was obtained hour by hour. As the circular slip method, the modified Fellenius method (Scott 1972; Kawamata et al. 2017) was used. The unit volume weight and the shear strength of the earth-fill dam and the foundation ground, both of which are required to conduct the circular slip calculation, were set based on the available geological survey and boring sampling results for each dam. Table 3 shows the test results. The damage probability was then calculated based on the return period. For the latter damage probability, the flood inflow at each dam was calculated using Eqs. 2 and 3 (MAFF 2004), and the probability that the flood inflow would exceed the discharge capacity of the spillway was calculated based on the return period at the dam site.

$$\varrho_p = \frac{r_e \cdot A}{3.6} \quad (2)$$

$$r_e = f_p \cdot r \quad (3)$$

where  $Q_p$ : flood inflow ( $\text{m}^3/\text{s}$ ),  $A$ : catchment area ( $\text{km}^2$ ),  $r_e$ : mean effective strength within the flood concentration time ( $\text{mm}/\text{hr}$ ),  $r$ : maximum rainfall intensity ( $\text{mm}/\text{hr}$ ), and  $f_p$ : peak runoff coefficient

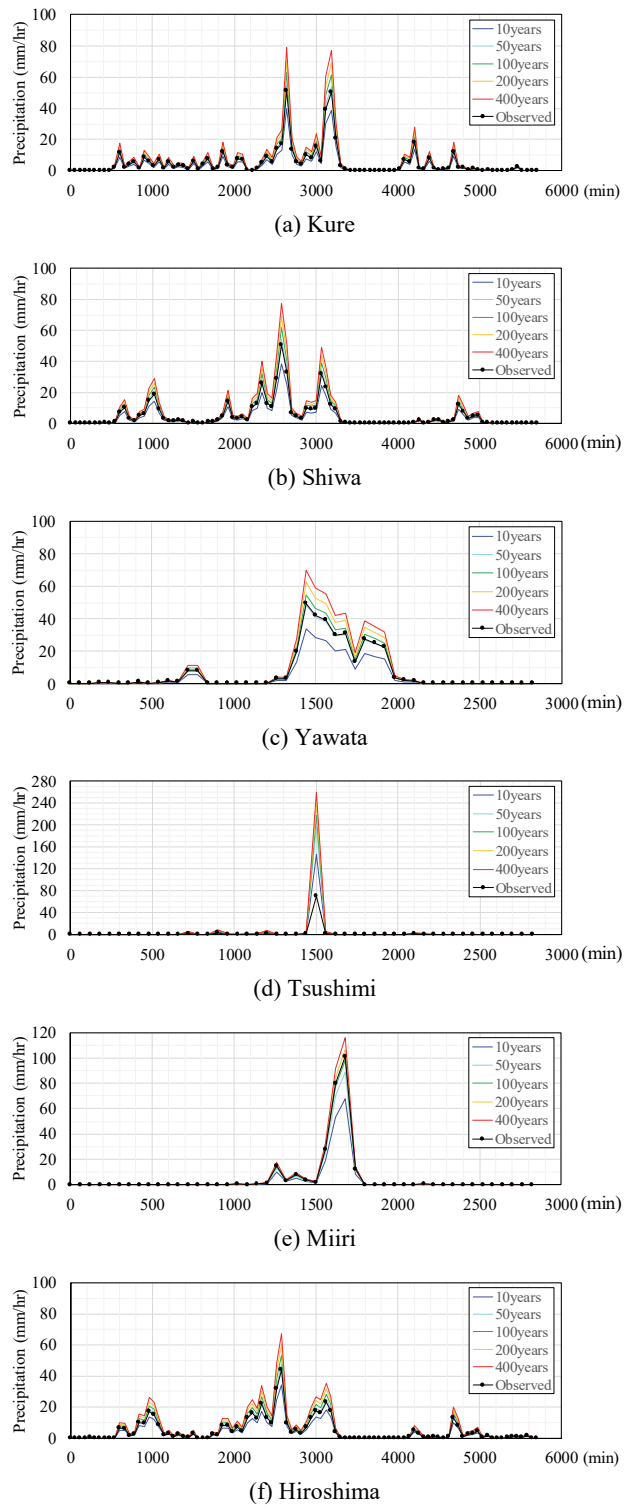


Figure 3. Time history of precipitation at each observatory

Table 3. Soil properties of each dam

	Unit weight (kN/m <sup>3</sup> )	Cohesion (kN/m <sup>2</sup> )	Internal friction angle (°)	Permeability (m/s)
A dam	20.8	35.9	17.1	$8.60 \times 10^{-6}$
B dam	18.5	7.8	29.6	$4.30 \times 10^{-6}$
C dam	19.8	5.1	37.1	$1.99 \times 10^{-7}$
D dam	19.3	11.2	36.7	$3.00 \times 10^{-8}$
E dam	19.5	8.2	38.5	$1.70 \times 10^{-7}$
F dam	19.4	17.1	32.2	$4.80 \times 10^{-8}$
G dam	18.9	17.3	30.7	$3.30 \times 10^{-8}$
H dam	19.2	13.4	32.8	$1.33 \times 10^{-7}$
I dam	17.8	11.0	32.3	$9.60 \times 10^{-6}$
J dam	20.4	30.1	30.2	$2.00 \times 10^{-7}$

The flood inflow at each dam was calculated using the probability of hourly precipitation for each site. The precipitation was calculated by the same method as that used for the daily probability of precipitation, but a probability distribution curve for the maximum hourly precipitation was employed. The probabilistic hourly rainfall in each return period was set as the maximum rainfall intensity ( $r$ ) in Eq. 3. Table 4 shows the flood inflow and discharge capacity of the spillway at each dam. For the discharge capacity of the spillway, the registered value for each dam was referred to. In the case of D dam, the existence of a spillway could not be confirmed.

Table 4. Calculated flood inflow at each dam

Discharge capacity (m <sup>3</sup> /s)	Q <sub>p</sub> (m <sup>3</sup> /s)				
	10 years	50 years	100 years	200 years	400 years
A dam	1.96	3.73	4.89	5.38	5.87
B dam	2.85	2.33	3.05	3.36	3.67
C dam	25.40	27.90	34.20	36.61	38.79
D dam	-	8.83	11.17	12.16	13.13
E dam	3.04	2.62	3.66	4.14	4.62
F dam	0.23	8.89	12.04	13.37	14.67
G dam	11.30	2.77	3.64	4.01	4.37
H dam	11.45	6.50	8.55	9.42	10.27
I dam	23.27	0.32	0.40	0.43	0.45
J dam	3.00	0.12	0.15	0.17	0.18

### 3. Results and Discussions

#### 3.1 Damage Probability of Slip Failure

As an example of the calculation results for the slope stability analysis, Figs. 4 and 5 show the cross section of I dam to be examined and the time history of the slope safety factor, respectively. In the case of I dam, the slope safety factor becomes the lowest at the second peak of the probabilistic hyetograph after the highest peak. The safety factor decreases when the return period increases and it reaches the lowest value in a shorter time. Fig. 6 shows the changes in the level of the water table inside the earth-fill dam for representative times and also the slip circle for which the minimum slope safety factor is obtained. This figure also shows that the level of the water table inside the earth-fill dam gradually rises from the downstream side of the dam embankment due to rainwater infiltration. When the water table rises to

almost the crest, at the time of 3,420 minutes, the slope safety factor of the earth-fill dam becomes less than 1.0.

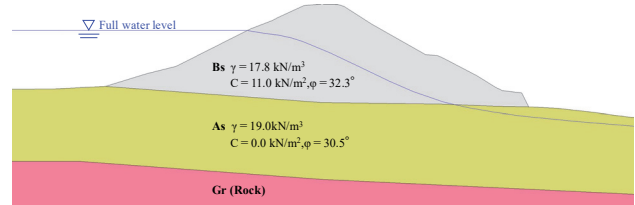


Figure 4. Analysis cross section (I dam)

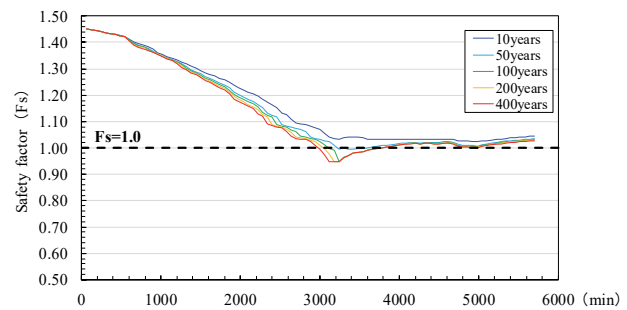


Figure 5. Time histories of slope safety factor (I dam)

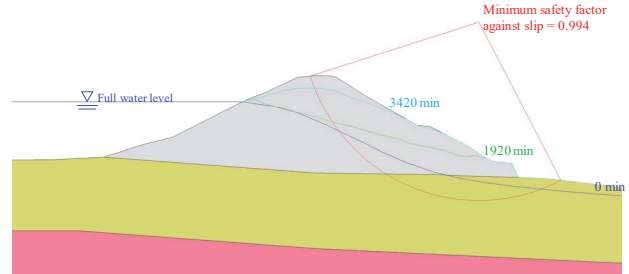


Figure 6. Seepage water table and circular slip line (I dam)

Table 5 shows the minimum slope safety factor for each return period of each small earth-fill dam. Only I dam has a safety factor lower than 1.0; the safety factor for all other dams exceeds 1.0 even for the rainfall of the return period of 400 years. There are two reasons for this: compared to the other dams, (i) I dam has relatively high permeability, which can make it easier for rainwater to infiltrate, and (ii) the shear strengths of this earth-fill dam and the foundation ground are relatively low.

Table 5. Minimum safety factor of each dam

	Hyetograph	Minimum safety factor against slip				
		10 years	50 years	100 years	200 years	400 years
A dam	Kure	1.819	1.807	1.807	1.807	1.807
B dam	Kure	1.401	1.361	1.343	1.333	1.325
C dam	Shiwa	1.638	1.636	1.635	1.632	1.631
D dam	Yawata	2.791	2.790	2.790	2.790	2.790
E dam	Tsushima	1.407	1.349	1.344	1.340	1.337
F dam	Miiri	1.372	1.372	1.372	1.371	1.371
G dam	Hiroshima	1.295	1.294	1.294	1.294	1.294
H dam	Hiroshima	1.475	1.474	1.474	1.474	1.474
I dam	Shiwa	1.023	0.994	0.949	0.949	0.949
J dam	Kure	2.07	2.07	2.069	2.069	2.069

### 3.2 Damage Probability of Overflow

Table 4 shows that the discharge capacity of the spillway is larger than the inflow corresponding to the return period of 400 years in four of the 10 dams. Fig. 7 shows the relationship between the return period and the flood inflow for the remaining six dams. This figure presents the return periods corresponding to the flood inflow equal to the discharge capacity of the spillway. The dots in Fig. 7 indicate the return period when the flood inflow reaches the discharge capacity of the spillway. In the cases of *A dam* and *F dam*, the calculated return period is less than one year. For *D dam*, it is not possible to evaluate the discharge capacity, since the capacity of the spillway cannot be identified.

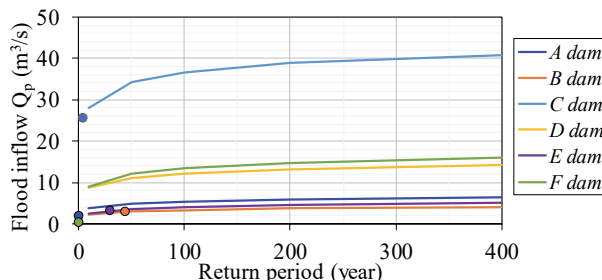


Figure 7. Correlation between flood inflow and return period

### 3.3 Summary of Damage Probability for Each Dam

Table 6 summarizes the damage probability for both slip failure and overflow. For only one of the 10 dams, namely, *I dam*, the damage probability due to slip failure is determined by the slip failure method. The table shows that damage may occur with the precipitation corresponding to a return period of 50 years. In contrast, for six of the 10 dams, the damage probability due to overflow is determined. It can be understood from the results that overflow is the more dominant factor, rather than slip failure, for damage to small earth-fill dams. The return period corresponding to the flood inflow equal to the discharge capacity of the spillway, as shown in Fig. 7, is used to determine the damage probability for overflow. Since the return period is less than one year for *A dam* and the capacity of the spillway is not clear for *D dam*, the return period is assumed to be one year. For the remaining four dams, it is predicted that they will not experience damage even due to precipitation corresponding to the return period of 400 years.

Table 6. Damage probability at each dam

	Hyetograph	Damage probability	
		Slip	Overflow
<i>A dam</i>	Kure	1/400	1/1
<i>B dam</i>	Kure	1/400	1/45
<i>C dam</i>	Shiwa	1/400	1/5
<i>D dam</i>	Yawata	1/400	1/1
<i>E dam</i>	Tsushima	1/400	1/30
<i>F dam</i>	Miiri	1/400	1/1
<i>G dam</i>	Hiroshima	1/400	1/400
<i>H dam</i>	Hiroshima	1/400	1/400
<i>I dam</i>	Shiwa	1/50	1/400
<i>J dam</i>	Kure	1/400	1/400

### 4. Conclusions

The following conclusions have been obtained from the series of analyses and considerations presented in this study.

- The results of the circular slip calculation, which took the infiltration of rainfall into consideration, suggest that only one of the 10 dams shows the possibility for the occurrence of slip failure.
- The probabilistic precipitation has exceeded the discharge capacity at six of the 10 targeted dams. These results mean that overflow is the more dominant factor, rather than slip failure, for damage to small earth-fill dams.

Based on the results of a series of calculations, etc., the damage probability was calculated for each of the 10 targeted dams. The priority of safeguarding measures for small earth-fill dams has conventionally tended to be determined by referring to the damage in the downstream area, which is predicted based on the assumption that dam breaching occurs as a deterministic event. The approach proposed here for a priority evaluation adds the concept of the damage probability of individual dams, following the concept of risk evaluation.

### Acknowledgement

This work was supported by a Grant-in-Aid for Scientific Research (A), Grant Number 16H02577, of the Japanese Society for the Promotion of Science (JSPS). This support is gratefully acknowledged.

### References

- Hori, T. 2005. Damage of Small Earth Dams for Irrigation Induced by Heavy Rainfall. In *Bulletin of the National Institute for Rural Engineering*, Japan, Vol. 44, pp. 139–247.
- Kawamata, H., Takenobu, M. and Miyata, M. 2017. A basic study of the Level 1 Reliability-based design method of circular slip failure verification by modified Fellenius' method. In *TECHNICAL NOTE of National Institute for Land and Infrastructure Management*, Japan, No. 955.
- Ministry of Agriculture, Forestry and Fisheries. 2018. How to lead future reservoir measures on the basis of The Heavy Rain Event of July 2018. In *Press Release of MAFF*, Japan, November 13, 2018.
- Ministry of Agriculture, Forestry and Fisheries. 2004. Design and Planning Criteria for Land Improvement Project “Dam Design”, Japan, pp. I-346–I-389.
- Ministry of Land, Infrastructure and Transport. 2014. Technical Criteria for River Works: Practical Guide for Research, Japan, Chapter 3-1, pp. 4–12.
- Scott, R.F. 1972. *Principles of Soil Mechanics*. Addison Wesley, p. 431.
- Takara, K. and Takasao, T. 1988. Criteria for evaluating probability distribution models in hydrologic frequency analysis. In *Journal of JSCE*, Vol. 393, II-9, pp. 151–160.